Journal of Systems Engineering and Electronics
Vol. 28, No. 6, December 2017, pp.1046 – 1056

DOA estimation for mixed signals with gain-phase error array

Jiaqi Zhen* and Yong Liu

College of Electronic Engineering, Heilongjiang University, Harbin 150080, China

Abstract: Most of the direction of arrival (DOA) estimation methods often need the exact array manifold, but in actual applications, the gain and phase of the channels are usually inconsistent, which will cause the estimation invalid. A novel direction finding approach for mixed far-field and near-field signals with gain-phase error array is provided. Based on simplifying the space spectrum function by matrix transformation, DOA of far-field signals is obtained. Consequently, errors of the array are acquired according to the orthogonality of far-field signal subspace and noise subspace. Finally, DOA of near-field signals can be estimated. The method merely needs one-dimensional spectrum searching, so as to improve the computational efficiency on the premise of ensuring a certain accuracy, simulation results manifest the effectiveness of the method.

Keywords: direction of arrival (DOA), gain-phase errors, far-field signals, near-field signals.

DOI: 10.21629/JSEE.2017.06.02

1. Introduction

Direction of arrival (DOA) estimation is a popular subject in signal processing, it is widely used in acoustic signal processing [1 – 6], internet of things [7 – 10] and electronic countermeasure [11 – 16]. At present, most of the methods are based on learning the accurate array manifold, however, the gain-phase of the channels are usually inconsistent in applications, which will cause the estimation invalid, so the array is necessary to be calibrated.

Generally speaking, there are two kinds of calibration methods: one is using source, the other is self correction. The former is implemented by using the auxiliary source whose position is known; the latter is often based on some iteration techniques to estimate the DOA and uncertainty parameters of the array alternately. Some of them have their unique superiorities. Liu [17] proposed an eigenstructure method which simultaneously estimated the DOA and gain-phase errors without joint iteration. Chen [18] studied the performance of near-field subband beamformers for arbitrary arrays in the presence of microphone gain and phase errors from the perspective of statistical analysis. Nikoofard [19] employed a dual-loop feedback which looks for the minimum gain-phase errors using a two-dimensional analog-based search algorithm and then finds the minimum value for the phase and gain mismatches. Dai [20] proposed an offline calibration algorithm for sensor gain-phase errors using two auxiliary sources, it is not necessary to know the accurate direction measurement of calibration sources. In the past few years, gain-phase calibration methods for the bistatic multiple-input multiple-output radar have raised [21 – 23], they also greatly promoted the practical application of corresponding techniques.

In the past ten years, some scholars have proposed some direction finding methods of mixed far-field and near-field signals (FS and NS) [24 – 30]. Liang [24] developed a two-stage multiple signal classification (MUSIC) algorithm using cumulant technique, it avoided two-dimensional search and pairing parameters. Wang [25] addressed a new mixed NS and FS localization algorithm based on sparse signal recovery, it can provide an improved estimation accuracy comparing with the past algorithms. He [26] derived the stochastic Cramer-Rao bound for scenarios where both the far-field and near-field narrowband sources may coexist. Liu [27] used an efficient third-order cyclic moment-based estimation of signal parameters via the rotational invariance techniques algorithm to cope with the mixed far-field and near-field cyclostationary sources location problem, and it avoided pairing parameters. Leong [28] proposed a technique for active detection and estimation of the

Manuscript received December 05, 2016.
*Corresponding author.
This work was supported by the National Natural Science Foundation of China (61501176; 61505050), the University Nursing Program for Young Scholars with Creative Talents in Heilongjiang Province (UNPYSCT-2016017), the Natural Science Foundation of Heilongjiang Province (F2015015), the Outstanding Young Scientist Foundation of Heilongjiang University (JCL201504), the China Postdoctoral Science Foundation (2014M561381), the Postdoctoral Foundation of Heilongjiang Province (LBH-Z14178), and the Special Research Funds for the Universities of Heilongjiang Province (HDRCCX-2016Z10).

range, radial velocity and DOA of multiple moving closely spaced targets in the three-dimensional space for both far-field and near-field cases. Zhang [29] optimized a beam-former pattern for far-field detection by maximizing the beam-former output in the direction of the far-field targets with the imposed condition to eliminate interfering signals from near-field locations. Based on the polynomial decomposing method and high-order cumulant technique, Wang [30] estimated DOA of these signals without any spectral search and parameter matching procedure. Malyuskin [31] studied the superdirective radiation patterns of ultracompact retrodirective antenna arrays, which improved the capability of distinguishing mixed signals. However there are rare published literature of the mixed signals with gain-phase error array.

A novel approach for direction finding of mixed FS and NS based on the gain-phase error array is provided in this paper. First, DOA of FS is obtained by simplifying the space spectrum function with matrix transformation. Then gain-phase errors are estimated, thus the array can be calibrated. Finally, DOA of NS is calculated, their locations can also be acquired in the open environment, this method merely needs one-dimensional spectrum searching, so as to improve the computation efficiency on the premise of ensuring a certain accuracy.

2. Signal model

2.1 Ideal signal model

Assume that there is a uniform linear array with $2M+1$ omnidirectional sensors, the 0th sensor is defined as the reference (origin), as shown in Fig. 1, N_1 narrowband FS and N_2 NS with the same frequency f and power impinge on the array simultaneously, they are $s_{n_1}(t)$ $(n_1 = 1,2,\dots,N_1)$ and $s_{n_2}(t)$ $(n_2 = 1,2,\dots,N_2)$, DOA of the them are $\boldsymbol{\theta} = [\theta_1,\dots,\theta_{N_1},\theta_{N_1+1},\dots,\theta_N]$ where $N = N_1+N_2$, $0<\theta<\pi$, the space of sensors is $d=\lambda/2$, λ is the corresponding wavelength of these signals.

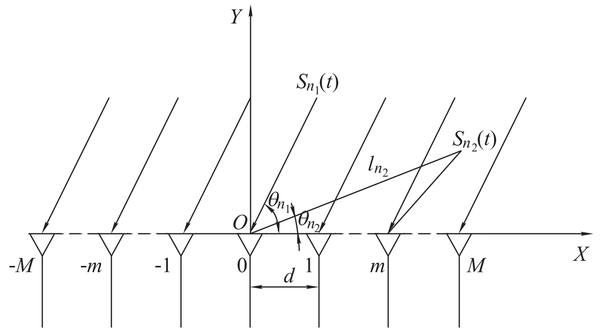

Fig. 1 Signal model

Here N_1, N_2 is known in advance, these signals are uncorrelated with one another, the distance of $s_{n_2}(t)$ to the origin is l_{n_2}, if observed time is T, the number of snapshots is Z, the received data by the array at time t_z $(z=1,2,\dots,Z)$ is expressed as

$$\boldsymbol{X}(t_z) = \begin{bmatrix} x_{-M}(t_z) \\ \vdots \\ x_{-m}(t_z) \\ \vdots \\ x_0(t_z) \\ \vdots \\ x_m(t_z) \\ \vdots \\ x_M(t_z) \end{bmatrix} = \begin{bmatrix} \sum_{n=1}^{N} s_n(t_z-\tau_{-M}(\theta_n)) \\ \vdots \\ \sum_{n=1}^{N} s_n(t_z-\tau_{-m}(\theta_n)) \\ \vdots \\ \sum_{n=1}^{N} s_n(t_z) \\ \vdots \\ \sum_{n=1}^{N} s_n(t_z-\tau_{m}(\theta_n)) \\ \vdots \\ \sum_{n=1}^{N} s_n(t_z-\tau_{M}(\theta_n)) \end{bmatrix} + \begin{bmatrix} e_{-M}(t_z) \\ \vdots \\ e_{-m}(t_z) \\ \vdots \\ e_0(t_z) \\ \vdots \\ e_m(t_z) \\ \vdots \\ e_M(t_z) \end{bmatrix}. \tag{1}$$

Then output of Z snapshots can be abbreviated

$$\boldsymbol{X} = \boldsymbol{A}(\theta)\boldsymbol{S} + \boldsymbol{E} \tag{2}$$

where $\boldsymbol{X} = [\boldsymbol{X}(t_1),\dots,\boldsymbol{X}(t_z),\dots,\boldsymbol{X}(t_Z)]$, $\boldsymbol{A}(\theta)$ is the array manifold with dimension $(2M+1)\times N$:

$$\begin{aligned}\boldsymbol{A}(\theta) = [&\boldsymbol{a}_{\mathrm{FS}}(\theta_1),\dots,\boldsymbol{a}_{\mathrm{FS}}(\theta_{n_1}),\dots,\boldsymbol{a}_{\mathrm{FS}}(\theta_{N_1}),\\ &\boldsymbol{a}_{\mathrm{NS}}(\theta_{N_1+1}),\dots,\boldsymbol{a}_{\mathrm{NS}}(\theta_{n_2}),\dots,\boldsymbol{a}_{\mathrm{NS}}(\theta_N)] = \\ &[\boldsymbol{A}_{\mathrm{FS}},\boldsymbol{A}_{\mathrm{NS}}]\end{aligned} \tag{3}$$

where $\boldsymbol{A}_{\mathrm{FS}} = [\boldsymbol{a}_{\mathrm{FS}}(\theta_1),\dots,\boldsymbol{a}_{\mathrm{FS}}(\theta_{n_1}),\dots,\boldsymbol{a}_{\mathrm{FS}}(\theta_{N_1})]$ is the array manifold of FS in ideal conditions, and $\boldsymbol{a}_{\mathrm{FS}}(\theta_{n_1})$ is the steering vector of $s_{n_1}(t)$; $\boldsymbol{A}_{\mathrm{NS}} = [\boldsymbol{a}_{\mathrm{NS}}(\theta_{N_1+1}),\dots,\boldsymbol{a}_{\mathrm{NS}}(\theta_{n_2}),\dots,\boldsymbol{a}_{\mathrm{NS}}(\theta_N)]$ is the array manifold of NS in ideal conditions, and $\boldsymbol{a}_{\mathrm{NS}}(\theta_{n_2})$ is the steering vector of $s_{n_2}(t)$, where

$$\begin{aligned}\boldsymbol{a}_{\mathrm{FS}}(\theta_{n_1}) = [&\exp(-\mathrm{j}2\pi f\tau_{-M}(\theta_{n_1})),\dots,\\ &\exp(-\mathrm{j}2\pi f\tau_{-m}(\theta_{n_1})),\dots,1,\dots,\\ &\exp(-\mathrm{j}2\pi f\tau_{m}(\theta_{n_1})),\dots,\exp(-\mathrm{j}2\pi f\tau_{M}(\theta_{n_1}))]^{\mathrm{T}}.\end{aligned} \tag{4}$$

And

$$\begin{aligned}&\tau_m(\theta_{n_1}) = m\frac{d}{c}\cos\theta_{n_1},\\ &m=-M,\dots,-m,\dots,0,\dots,m,\dots,M;\\ &n_1 = 1,2,\dots,N_1\end{aligned} \tag{5}$$

is the delay for $s_{n_1}(t)$ arriving at the mth sensor with respect to the origin, c is the speed of the signal, we also have

$$\boldsymbol{a}_{\mathrm{NS}}(\theta_{n_2}) = [\exp(-\mathrm{j}2\pi f\tau_{-M}(\theta_{n_2})),\dots,$$

$$\exp(-\mathrm{j}2\pi f\tau_{-m}(\theta_{n_2})),\dots,1,\dots,$$
$$\exp(-\mathrm{j}2\pi f\tau_m(\theta_{n_2})),\dots,\exp(-\mathrm{j}2\pi f\tau_M(\theta_{n_2}))]^{\mathrm{T}}. \quad (6)$$

Combing the cosine law, we can deduce $\tau_m(\theta_{n_2})$ from geometrical relationship in Fig. 1.

$$\tau_m(\theta_{n_2}) = \frac{l_{n_2} - \sqrt{l_{n_2}^2 + (md)^2 - 2l_{n_2}md\cos\theta_{n_2}}}{c}. \quad (7)$$

It is the delay for $s_{n_2}(t)$ arriving at the mth sensor with respect to the origin, Fourier series [32] is employed for expanding (7).

$$\tau_m(\theta_{n_2}) = \frac{m^2d^2}{4l_{n_2}c}\cos(2\theta_{n_2}) + \frac{1}{c}md\cos\theta_{n_2} - \frac{m^2d^2}{4l_{n_2}c}. \quad (8)$$

In (2), we have

$$\boldsymbol{S} = [\boldsymbol{S}_{\mathrm{FS}}, \boldsymbol{S}_{\mathrm{NS}}]^{\mathrm{T}} = [\boldsymbol{S}_1,\dots,\boldsymbol{S}_{n_1},\dots,$$
$$\boldsymbol{S}_{N_1}, \boldsymbol{S}_{N_1+1},\dots,\boldsymbol{S}_{n_2},\dots,\boldsymbol{S}_N]^{\mathrm{T}}. \quad (9)$$

It is the signal vector, $[\ ]^{\mathrm{T}}$ means the transpose of $[\ ]$, where $\boldsymbol{S}_{\mathrm{FS}} = [\boldsymbol{S}_1,\dots,\boldsymbol{S}_{n_1},\dots,\boldsymbol{S}_{N_1}]^{\mathrm{T}}$ is the vector of FS, $\boldsymbol{S}_{\mathrm{NS}} = [\boldsymbol{S}_{N_1+1},\dots,\boldsymbol{S}_{n_2},\dots,\boldsymbol{S}_N]^{\mathrm{T}}$ is that of NS. $\boldsymbol{E}$ is the Gaussian white noise matrix with mean 0 and variance σ^2, then the covariance matrix in ideal conditions is

$$\boldsymbol{R} = \frac{1}{Z}\boldsymbol{X}\boldsymbol{X}^{\mathrm{H}} =$$
$$\frac{1}{Z}\boldsymbol{A}(\theta)\boldsymbol{S}\boldsymbol{S}^{\mathrm{H}}\boldsymbol{A}^{\mathrm{H}}(\theta) + \sigma^2\boldsymbol{I}_{(2M+1)\times(2M+1)} =$$
$$\boldsymbol{R}_{\mathrm{FS}} + \boldsymbol{R}_{\mathrm{NS}} + \sigma^2\boldsymbol{I}_{(2M+1)\times(2M+1)}. \quad (10)$$

Here, $\boldsymbol{X}^{\mathrm{H}}$ denotes the conjugate transpose of $\boldsymbol{X}$, the covariance matrix of FS is $\boldsymbol{R}_{\mathrm{FS}} = \frac{1}{Z}\boldsymbol{A}_{\mathrm{FS}}\boldsymbol{S}_{\mathrm{FS}}\boldsymbol{S}_{\mathrm{FS}}^{\mathrm{H}}\boldsymbol{A}_{\mathrm{FS}}^{\mathrm{H}}$, and that of NS is $\boldsymbol{R}_{\mathrm{NS}} = \frac{1}{Z}\boldsymbol{A}_{\mathrm{NS}}\boldsymbol{S}_{\mathrm{NS}}\boldsymbol{S}_{\mathrm{NS}}^{\mathrm{H}}\boldsymbol{A}_{\mathrm{NS}}^{\mathrm{H}}$.

2.2 Error model

The gain-phase errors can be modeled by

$$\boldsymbol{W} = \mathrm{diag}([W_{-M},\dots,W_{-m},\dots,1,\dots,$$
$$W_m,\dots,W_M]^{\mathrm{T}}) \quad (11)$$

where $\mathrm{diag}(\ )$ means forming a diagonal matrix by taking the given vector as main diagonal, and

$$W_m = \rho_m \mathrm{e}^{\mathrm{j}\phi_m},\ \ m \in [-M, M] \quad (12)$$

is the gain-phase errors of the mth channel, ρ_m, ϕ_m are respectively the gain and phase of the mth channel with respect to the reference, thus the steering vector of the nth signal at present is

$$\boldsymbol{a}'(\theta_n) = [W_{-M}\mathrm{e}^{-\mathrm{j}2\pi f\tau_{-M}(\theta_n)},\dots,$$
$$W_{-m}\mathrm{e}^{-\mathrm{j}2\pi f\tau_{-m}(\theta_n)},\dots,1,\dots,W_m\mathrm{e}^{-\mathrm{j}2\pi f\tau_m(\theta_n)},\dots,$$
$$W_M\mathrm{e}^{-\mathrm{j}2\pi f\tau_M(\theta_n)}]^{\mathrm{T}} = \mathrm{diag}([W_{-M},\dots,W_{-m},\dots,$$
$$1,\dots,W_m,\dots,W_M]^{\mathrm{T}})\boldsymbol{a}(\theta_n) =$$
$$\boldsymbol{W}\boldsymbol{a}(\theta_n),\ \ n = 1,2,\dots,N. \quad (13)$$

The corresponding array manifold is

$$\boldsymbol{A}'(\theta) = [\boldsymbol{a}'_{\mathrm{FS}}(\theta_1),\dots,\boldsymbol{a}'_{\mathrm{FS}}(\theta_{n_1}),\dots,\boldsymbol{a}'_{\mathrm{FS}}(\theta_{N_1}),$$
$$\boldsymbol{a}'_{\mathrm{NS}}(\theta_{N_1+1}),\dots,\boldsymbol{a}'_{\mathrm{NS}}(\theta_{n_2}),\dots,\boldsymbol{a}'_{\mathrm{NS}}(\theta_N)] =$$
$$[\boldsymbol{A}'_{\mathrm{FS}}, \boldsymbol{A}'_{\mathrm{NS}}] = \boldsymbol{W}\boldsymbol{A}(\theta) \quad (14)$$

where

$$\boldsymbol{A}'_{\mathrm{FS}} = \boldsymbol{W}\boldsymbol{A}_{\mathrm{FS}} =$$
$$[\boldsymbol{a}'_{\mathrm{FS}}(\theta_1),\dots,\boldsymbol{a}'_{\mathrm{FS}}(\theta_{n_1}),\dots,\boldsymbol{a}'_{\mathrm{FS}}(\theta_{N_1})]$$

is the array manifold of FS, $\boldsymbol{a}'_{\mathrm{FS}}(\theta_{n_1})$ is the corresponding steering vector of $s_{n_1}(t)$;

$$\boldsymbol{A}'_{\mathrm{NS}} = \boldsymbol{W}\boldsymbol{A}_{\mathrm{NS}} =$$
$$[\boldsymbol{a}'_{\mathrm{NS}}(\theta_{N_1+1}),\dots,\boldsymbol{a}'_{\mathrm{NS}}(\theta_{n_2}),\dots,\boldsymbol{a}'_{\mathrm{NS}}(\theta_N)]$$

is the array manifold of NS, $\boldsymbol{a}'_{\mathrm{NS}}(\theta_{n_2})$ is the corresponding steering vector of $s_{n_2}(t)$, and the output in the presence of gain-phase errors is

$$\boldsymbol{X}' = \boldsymbol{A}'(\theta)\boldsymbol{S} + \boldsymbol{E} = \boldsymbol{W}\boldsymbol{A}(\theta)\boldsymbol{S} + \boldsymbol{E}. \quad (15)$$

3. Proposed method

3.1 DOA estimation of FS

First, the covariance matrix in the presence of gain-phase errors can be acquired

$$\boldsymbol{R}' = \frac{1}{Z}\boldsymbol{X}'(\boldsymbol{X}')^{\mathrm{H}} =$$
$$\frac{1}{Z}\boldsymbol{A}'(\theta)\boldsymbol{S}\boldsymbol{S}^{\mathrm{H}}(\boldsymbol{A}'(\theta))^{\mathrm{H}} + \sigma^2\boldsymbol{I}_{(2M+1)\times(2M+1)} =$$
$$\frac{1}{Z}\boldsymbol{W}\boldsymbol{A}(\theta)\boldsymbol{S}\boldsymbol{S}^{\mathrm{H}}\boldsymbol{A}^{\mathrm{H}}(\theta)\boldsymbol{W}^{\mathrm{H}} + \sigma^2\boldsymbol{I}_{(2M+1)\times(2M+1)} =$$
$$\boldsymbol{R}'_{\mathrm{FS}} + \boldsymbol{R}'_{\mathrm{NS}} + \sigma^2\boldsymbol{I}_{(2M+1)\times(2M+1)} \quad (16)$$

where the covariance matrix of the FS in the presence of gain and phase error is $\boldsymbol{R}'_{\mathrm{FS}} = \frac{1}{Z}\boldsymbol{W}\boldsymbol{A}_{\mathrm{FS}}\boldsymbol{S}_{\mathrm{FS}}\boldsymbol{S}_{\mathrm{FS}}^{\mathrm{H}}\boldsymbol{A}_{\mathrm{FS}}^{\mathrm{H}}\boldsymbol{W}^{\mathrm{H}}$, that of the NS is $\boldsymbol{R}'_{\mathrm{NS}} = \frac{1}{Z}\boldsymbol{W}\boldsymbol{A}_{\mathrm{NS}}\boldsymbol{S}_{\mathrm{NS}}\boldsymbol{S}_{\mathrm{NS}}^{\mathrm{H}}\boldsymbol{A}_{\mathrm{NS}}^{\mathrm{H}}\boldsymbol{W}^{\mathrm{H}}$. We can acquire the eigenvector $\boldsymbol{U}' = [\boldsymbol{U}'_S\boldsymbol{U}'_E]$ by decomposing $\boldsymbol{R}'$, here $\boldsymbol{U}'_S$ is the signal eigenvector and $\boldsymbol{U}'_E$ is the noise eigenvector, then combining MUSIC algorithm [33], we can establish the following spatial spectrum of FS,

$$P_{MU-F}(\theta) = \frac{1}{(\boldsymbol{a}'_{\mathrm{FS}}(\theta))^{\mathrm{H}}\boldsymbol{U}'_E(\boldsymbol{U}'_E)^{\mathrm{H}}\boldsymbol{a}'_{\mathrm{FS}}(\theta)} =$$
$$\frac{1}{\boldsymbol{a}_{\mathrm{FS}}^{\mathrm{H}}(\theta)\boldsymbol{W}^{\mathrm{H}}\boldsymbol{U}'_E(\boldsymbol{U}'_E)^{\mathrm{H}}\boldsymbol{W}\boldsymbol{a}_{\mathrm{FS}}(\theta)} = \frac{1}{Y}. \quad (17)$$

The denominator of (17) can be transformed into

$$Y = \sum_{n_1=1}^{N_1} \boldsymbol{a}_{\mathrm{FS}}^{\mathrm{H}}(\theta_{n_1})\boldsymbol{W}^{\mathrm{H}}\boldsymbol{U}_E'(\boldsymbol{U}_E')^{\mathrm{H}}\boldsymbol{W}\boldsymbol{a}_{\mathrm{FS}}(\theta_{n_1}). \quad (18)$$

Define the gain-phase error vector

$$\boldsymbol{w} = [\rho_{-M}\mathrm{e}^{\mathrm{j}\phi_{-M}}, \dots, \rho_{-m}\mathrm{e}^{\mathrm{j}\phi_{-m}}, \dots, 1, \dots, \rho_m\mathrm{e}^{\mathrm{j}\phi_m}, \dots, \rho_M\mathrm{e}^{\mathrm{j}\phi_M}]^{\mathrm{T}}. \quad (19)$$

In fact, we can simplify Y further

$$Y = \sum_{n_1=1}^{N_1} \boldsymbol{a}_{\mathrm{FS}}^{\mathrm{H}}(\theta_{n_1})\boldsymbol{W}^{\mathrm{H}}\boldsymbol{U}_E'(\boldsymbol{U}_E')^{\mathrm{H}}\boldsymbol{W}\boldsymbol{a}_{\mathrm{FS}}(\theta_{n_1}) = \sum_{n_1=1}^{N_1} \boldsymbol{w}^{\mathrm{H}}\{(\mathrm{diag}(\boldsymbol{a}_{\mathrm{FS}}(\theta_{n_1})))^{\mathrm{H}}\boldsymbol{U}_E'(\boldsymbol{U}_E')^{\mathrm{H}}\cdot \mathrm{diag}(\boldsymbol{a}_{\mathrm{FS}}(\theta_{n_1}))\}\boldsymbol{w} = \boldsymbol{w}^{\mathrm{H}}\boldsymbol{B}(\theta)\boldsymbol{w} \quad (20)$$

where

$$\boldsymbol{B}(\theta) = \sum_{n_1=1}^{N_1} \{(\mathrm{diag}(\boldsymbol{a}_{\mathrm{FS}}(\theta_{n_1})))^{\mathrm{H}}\boldsymbol{U}_E'(\boldsymbol{U}_E')^{\mathrm{H}}\mathrm{diag}(\boldsymbol{a}_{\mathrm{FS}}(\theta_{n_1}))\}.$$

According to the MUSIC algorithm, DOA of FS can be estimated by minimizing (20). $\boldsymbol{w} \neq \boldsymbol{0}$, so $\boldsymbol{w}^{\mathrm{H}}\boldsymbol{B}(\theta)\boldsymbol{w}$ will be zero only if $\boldsymbol{B}(\theta)$ is singular, then we will calculate the estimation $\hat{\theta}_1, \dots \hat{\theta}_{N_1}$ by searching N_1 peaks of the following modified equation

$$P_{MMU-F}(\theta) = \frac{1}{|\boldsymbol{B}(\theta)|} \quad (21)$$

where $|\ \ |$ denotes solving determinant, thus, DOA of FS can be determined through one-dimensional searching without knowing gain-phase errors.

3.2 Estimation of gain-phase errors

The orthogonality of signal subspace of FS and noise subspace will be employed for estimating the gain-phase errors, that is

$$(\boldsymbol{a}_{\mathrm{FS}}'(\theta_{n_1}))^{\mathrm{H}}\boldsymbol{U}_E' = \boldsymbol{a}_{\mathrm{FS}}^{\mathrm{H}}(\theta_{n_1})\boldsymbol{W}^{\mathrm{H}}\boldsymbol{U}_E' = \boldsymbol{0}_{1\times(2M+1-N)}. \quad (22)$$

It is the same as

$$\boldsymbol{a}_{\mathrm{FS}}^{\mathrm{H}}(\theta_{n_1})\boldsymbol{W}^{\mathrm{H}}\boldsymbol{U}_E' = \boldsymbol{w}^{\mathrm{H}}\{\mathrm{diag}(\boldsymbol{a}_{\mathrm{FS}}(\theta_{n_1}))\}^{\mathrm{H}}\boldsymbol{U}_E' = \boldsymbol{w}^{\mathrm{H}}\boldsymbol{Q}(\theta_{n_1}). \quad (23)$$

Here $\boldsymbol{Q}(\theta_{n_1}) = \{\mathrm{diag}(\boldsymbol{a}_{\mathrm{FS}}(\theta_{n_1}))\}^{\mathrm{H}}\boldsymbol{U}_E'$, define $\boldsymbol{D}$ as the middle row of $\boldsymbol{U}_E'$, as the middle row of $\boldsymbol{a}_{\mathrm{FS}}(\theta_{n_1})$ equals 1, the middle element of $\boldsymbol{Q}(\theta_{n_1})$ is $\boldsymbol{D}$ too. Integrating all FS, let $\boldsymbol{Q}(\theta) = [\boldsymbol{Q}(\theta_1), \dots, \boldsymbol{Q}(\theta_{n_1}), \dots, \boldsymbol{Q}(\theta_{N_1})]$, we have

$$\boldsymbol{w}^{\mathrm{H}}\boldsymbol{Q}(\theta) = \boldsymbol{w}^{\mathrm{H}}\begin{bmatrix}\boldsymbol{Q}_1(\theta)\\ \boldsymbol{D}\cdots\boldsymbol{D}\\ \boldsymbol{Q}_2(\theta)\end{bmatrix}_{(2M+1)\times(2M+1-N)N_1} = [\boldsymbol{w}_1^{\mathrm{H}}, 1, \boldsymbol{w}_2^{\mathrm{H}}]\begin{bmatrix}\boldsymbol{Q}_1(\theta)\\ \boldsymbol{D}\cdots\boldsymbol{D}\\ \boldsymbol{Q}_2(\theta)\end{bmatrix}_{(2M+1)\times(2M+1-N)N_1} = [\boldsymbol{0}, \dots, \boldsymbol{0}]_{1\times(2M+1-N)N_1} \quad (24)$$

where $\boldsymbol{w}_1$ is the first M rows of $\boldsymbol{w}$, $\boldsymbol{w}_2$ is the latter M rows of $\boldsymbol{w}$, $\boldsymbol{Q}_1(\theta)$ is the first M rows of $\boldsymbol{Q}(\theta)$, $\boldsymbol{Q}_2(\theta)$ is the latter M rows of $\boldsymbol{Q}(\theta)$, define $\boldsymbol{G} = [\boldsymbol{D}\cdots\boldsymbol{D}]_{1\times(2M+1-N)N_1}$, $\boldsymbol{w}_1$ and $\boldsymbol{w}_2$ will be acquired according to (24), that is

$$\hat{\boldsymbol{w}}_1 = -(\boldsymbol{G} \times \mathrm{pinv}(\boldsymbol{Q}_1(\theta)))^{\mathrm{H}} \quad (25)$$

$$\hat{\boldsymbol{w}}_2 = -(\boldsymbol{G} \times \mathrm{pinv}(\boldsymbol{Q}_2(\theta)))^{\mathrm{H}}. \quad (26)$$

$\hat{\boldsymbol{w}}_1$ and $\hat{\boldsymbol{w}}_2$ is the estimation of $\boldsymbol{w}_1$ and $\boldsymbol{w}_2$, pinv( ) means solving pseudo-inverse, then we have

$$\hat{\boldsymbol{w}} = [\hat{\boldsymbol{w}}_1^{\mathrm{T}}, 1, \hat{\boldsymbol{w}}_2^{\mathrm{T}}]^{\mathrm{T}}. \quad (27)$$

Thus, estimation of $\boldsymbol{W}$ can also be acquired.

3.3 DOA estimation of NS

We can estimate the covariance matrix without the errors and noise according to (16)

$$\bar{\boldsymbol{R}} = \hat{\boldsymbol{W}}^{-1}(\boldsymbol{R}' - \sigma^2\boldsymbol{I}_{(2M+1)\times(2M+1)})(\hat{\boldsymbol{W}}^{\mathrm{H}})^{-1} = \bar{\boldsymbol{R}}_{\mathrm{FS}} + \bar{\boldsymbol{R}}_{\mathrm{NS}} \quad (28)$$

where $\hat{\boldsymbol{W}}$ is the estimation of $\boldsymbol{W}$, $\bar{\boldsymbol{R}}_{\mathrm{FS}}$ and $\bar{\boldsymbol{R}}_{\mathrm{NS}}$ are respectively the estimation of $\boldsymbol{R}_{\mathrm{FS}}$ and $\boldsymbol{R}_{\mathrm{NS}}$, σ^2 can be replaced by the minimum eigenvalue of $\boldsymbol{R}'$.

It is seen from (10), $\bar{\boldsymbol{R}}_{\mathrm{FS}}$ is a Hermitian matrix, and has Toeplitz property (Toeplitz means the elements on clinodiagonal line of the matrix is equal), and $\bar{\boldsymbol{R}}_{\mathrm{NS}}$ is a Hermitian matrix, but has no Toeplitz property.

Proof Define $\gamma_{\alpha,\beta}$ as the element of row α, column β in $\bar{\boldsymbol{R}}_{\mathrm{FS}}$, according to (10), we have

$$\gamma_{\alpha,\beta} = \mathrm{E}\left\{\left[\sum_{g=1}^{N_1}\boldsymbol{a}_{\mathrm{FS}-\alpha}(\theta_g)s_{n_1-g}(t_z)\right]\times\left[\sum_{h=1}^{N_1}\boldsymbol{a}_{\mathrm{FS}-\beta}^*(\theta_h)s_{n_1-h}^*(t_z)\right]\right\} + \mathrm{E}[e_\alpha(t_z)e_\beta^*(t_z)] = \left[\sum_{g=1}^{N_1}\mu^2\boldsymbol{a}_{\mathrm{FS}-\alpha}(\theta_g)\boldsymbol{a}_{\mathrm{FS}-\beta}^*(\theta_h)\right] + \sigma^2\delta_{\alpha,\beta} \quad (29)$$

where μ^2 is the signal power received by the array, $\boldsymbol{a}_{\mathrm{FS}-\alpha}(\theta_g)$ represents the element of row α, column g in $\boldsymbol{A}_{\mathrm{FS}}$, $s_{n_1-g}(t_z)$ means the zth samples of the gth FS, $\delta_{\alpha,\beta}$

denotes Dirac delta function, combining (4) and (5), we have

$$\boldsymbol{a}_{\mathrm{FS}-\alpha}(\theta_g)=\left\{-\mathrm{j}2\pi f\left(\alpha\frac{d}{c}\cos\theta_g\right)\right\}. \tag{30}$$

Thus

$$\gamma_{\alpha,\beta}=\left\{\sum_{g=1}^{N_1}\mu^2\exp\left[-\mathrm{j}2\pi f\left(\alpha\frac{d}{c}\cos\theta_g\right)\right]\times \exp\left[\mathrm{j}2\pi f\left(\beta\frac{d}{c}\cos\theta_g\right)\right]\right\}+\sigma^2\delta_{\alpha,\beta}= \left\{\sum_{g=1}^{N_1}\mu^2\exp\left[-\mathrm{j}2\pi f\left((\alpha-\beta)\frac{d}{c}\cos\theta_g\right)\right]\right\}+\sigma^2\delta_{\alpha,\beta}. \tag{31}$$

Similarly, element on row $\alpha+1$, column $\beta+1$ in $\bar{\boldsymbol{R}}_{\mathrm{FS}}$ is

$$\gamma_{\alpha+1,\beta+1}=\left\{\sum_{g=1}^{N_1}\mu^2\exp\left[-\mathrm{j}2\pi f\left((\alpha-\beta)\frac{d}{c}\cos\theta_g\right)\right]\right\}+\sigma^2\delta_{\alpha+1,\beta+1}. \tag{32}$$

Comparing (31) with (32), it can be concluded $\gamma_{\alpha,\beta}=\gamma_{\alpha+1,\beta+1}$, so $\bar{\boldsymbol{R}}_{\mathrm{FS}}$ has Toeplitz property.

In the same way, for $\bar{\boldsymbol{R}}_{\mathrm{NS}}$,

$$\gamma_{\alpha,\beta}=\mathrm{E}\left\{\left[\sum_{g=1}^{N_2}\boldsymbol{a}_{\mathrm{NS}-\alpha}(\theta_g)s_{n_2-g}(t_z)\right]\times \left[\sum_{h=1}^{N_2}\boldsymbol{a}^*_{\mathrm{NS}-\beta}(\theta_h)s^*_{n_2-h}(t_z)\right]\right\}+ \mathrm{E}[e_\alpha(t_z)e^*_\beta(t_z)]= \left[\sum_{g=1}^{N_2}\mu^2\boldsymbol{a}_{\mathrm{NS}-\alpha}(\theta_g)\boldsymbol{a}^*_{\mathrm{NS}-\beta}(\theta_h)\right]+\sigma^2\delta_{\alpha,\beta}. \tag{33}$$

According to (6) and (8), we have

$$\boldsymbol{a}_{\mathrm{NS}-\alpha}(\theta_g)= \exp\left\{-\mathrm{j}2\pi f\left[\frac{\alpha^2d^2}{4l_gc}\cos(2\theta_g)+\frac{1}{c}\alpha d\cos\theta_g-\frac{\alpha^2d^2}{4l_gc}\right]\right\}. \tag{34}$$

Thus

$$\gamma_{\alpha,\beta}=\left\{\sum_{g=1}^{N_2}\mu^2\exp\left[-\mathrm{j}2\pi f\left(\frac{\alpha^2d^2}{4l_gc}\cos(2\theta_g)+ \frac{1}{c}\alpha d\cos\theta_g-\frac{\alpha^2d^2}{4l_gc}\right)\right]\times\exp\left[\mathrm{j}2\pi f\left(\frac{\beta^2d^2}{4l_gc}\cos(2\theta_g)+ \frac{1}{c}\beta d\cos\theta_g-\frac{\beta^2d^2}{4l_gc}\right)\right]\right\}+\sigma^2\delta_{\alpha,\beta}= \left\{\sum_{g=1}^{N_2}\mu^2\exp\left[-\mathrm{j}2\pi f\left(\frac{(\alpha^2-\beta^2)d^2}{4l_gc}\cos(2\theta_g)+ \frac{1}{c}(\alpha-\beta)d\cos\theta_g-\frac{(\alpha^2-\beta^2)d^2}{4l_gc}\right)\right]\right\}+\sigma^2\delta_{\alpha,\beta}= \left\{\sum_{g=1}^{N_2}\mu^2\exp\left[-\mathrm{j}2\pi f\left(\left(\frac{(\alpha^2-\beta^2)d^2}{2l_gc}\times(\cos^2\theta_g-1)\right)+ \frac{1}{c}(\alpha-\beta)d\cos\theta_g\right)\right]\right\}+\sigma^2\delta_{\alpha,\beta}. \tag{35}$$

The element on row $\alpha+1$, column $\beta+1$ in $\bar{\boldsymbol{R}}_{\mathrm{NS}}$ is

$$\gamma_{\alpha+1,\beta+1}= \left\{\sum_{g=1}^{N_2}\mu^2\exp\left[-\mathrm{j}2\pi f\left(\left(\frac{((\alpha+1)^2-(\beta+1)^2)d^2}{2l_gc}\times (\cos^2\theta_g-1)\right)+\frac{1}{c}(\alpha-\beta)d\cos\theta_g\right)\right]\right\}+\sigma^2\delta_{\alpha+1,\beta+1}. \tag{36}$$

Comparing (35) with (36), in general, $\alpha^2-\beta^2\neq(\alpha+1)^2-(\beta+1)^2$, so $\gamma_{\alpha,\beta}\neq\gamma_{\alpha+1,\beta+1}$, thus, $\bar{\boldsymbol{R}}_{\mathrm{NS}}$ has no Toeplitz

Thus the covariance matrix of FS meets [34]:

$$\bar{\boldsymbol{R}}^{\mathrm{T}}_{\mathrm{FS}}=\boldsymbol{J}\bar{\boldsymbol{R}}_{\mathrm{FS}}\boldsymbol{J} \tag{37}$$

where $\boldsymbol{J}$ is a $(2M+1)\times(2M+1)$ dimensional anti-identity matrix with ones on its anti-diagonal and zeros elsewhere. The covariance matrix of NS satisfies:

$$\bar{\boldsymbol{R}}^{\mathrm{H}}_{\mathrm{NS}}=\bar{\boldsymbol{R}}_{\mathrm{NS}}. \tag{38}$$

Thus we can eliminate the information of FS in $\bar{\boldsymbol{R}}$, that is

$$\tilde{\boldsymbol{R}}=(\bar{\boldsymbol{R}}^{\mathrm{T}}-\boldsymbol{J}\bar{\boldsymbol{R}}\boldsymbol{J}))^*= ((\bar{\boldsymbol{R}}_{\mathrm{FS}}+\bar{\boldsymbol{R}}_{\mathrm{NS}})^{\mathrm{T}}-\boldsymbol{J}(\bar{\boldsymbol{R}}_{\mathrm{FS}}+\bar{\boldsymbol{R}}_{\mathrm{NS}})\boldsymbol{J})^*= (\bar{\boldsymbol{R}}^{\mathrm{T}}_{\mathrm{FS}}-\boldsymbol{J}\bar{\boldsymbol{R}}_{\mathrm{FS}}\boldsymbol{J})^*+(\bar{\boldsymbol{R}}^{\mathrm{T}}_{\mathrm{NS}}-\boldsymbol{J}\bar{\boldsymbol{R}}_{\mathrm{NS}}\boldsymbol{J})^*= \bar{\boldsymbol{R}}_{\mathrm{NS}}-\boldsymbol{J}\bar{\boldsymbol{R}}^*_{\mathrm{NS}}\boldsymbol{J}= \frac{1}{Z}\boldsymbol{A}_{\mathrm{NS}}\boldsymbol{S}_{\mathrm{NS}}\boldsymbol{S}^{\mathrm{H}}_{\mathrm{NS}}\boldsymbol{A}^{\mathrm{H}}_{\mathrm{NS}}-\frac{1}{Z}\boldsymbol{J}(\boldsymbol{A}_{\mathrm{NS}}\boldsymbol{S}_{\mathrm{NS}}\boldsymbol{S}^{\mathrm{H}}_{\mathrm{NS}}\boldsymbol{A}^{\mathrm{H}}_{\mathrm{NS}})^*\boldsymbol{J}. \tag{39}$$

Eigen-decomposition is performed on $\tilde{\boldsymbol{R}}$, the eigenvalue $\tilde{\boldsymbol{\Sigma}}$ and eigenvector $\tilde{\boldsymbol{U}}$ of $\tilde{\boldsymbol{R}}$ can be obtained, then we have

$$\boldsymbol{a}^{\mathrm{H}}_{\mathrm{NS}}(\theta)\tilde{\boldsymbol{U}}\tilde{\boldsymbol{U}}^{\mathrm{H}}\boldsymbol{a}_{\mathrm{NS}}(\theta)=0. \tag{40}$$

According to the characteristics of eigen-decomposition [34], $-\tilde{\boldsymbol{\Sigma}}$ and $\boldsymbol{J}\tilde{\boldsymbol{U}}^*$ are also the eigenvalue and eigenvector of $\tilde{\boldsymbol{R}}$, so

$$\boldsymbol{a}^{\mathrm{H}}_{\mathrm{NS}}(\theta)(\boldsymbol{J}\tilde{\boldsymbol{U}}^*)(\boldsymbol{J}\tilde{\boldsymbol{U}}^*)^{\mathrm{H}}\boldsymbol{a}_{\mathrm{NS}}(\theta)=0. \tag{41}$$

Take the conjugate of (41)

$$(\boldsymbol{a}_{\mathrm{NS}}^*(\theta))^{\mathrm{H}}(\boldsymbol{J}\tilde{\boldsymbol{U}})(\boldsymbol{J}\tilde{\boldsymbol{U}})^{\mathrm{H}}\boldsymbol{a}_{\mathrm{NS}}^*(\theta) = [\boldsymbol{J}\boldsymbol{a}_{\mathrm{NS}}^*(\theta)]^{\mathrm{H}}\tilde{\boldsymbol{U}}\tilde{\boldsymbol{U}}^{\mathrm{H}}[\boldsymbol{J}\boldsymbol{a}_{\mathrm{NS}}^*(\theta)] = 0. \tag{42}$$

From (6) and (7), we know $\boldsymbol{a}_{\mathrm{NS}}(\theta)$ includes the information of the distance and DOA, it will be two-dimensional searching if we use the MUSIC algorithm directly, it is necessary to reduce the computation by the matrix transformation based on the array structure. In (40) and (42), we respectively have $\boldsymbol{a}_{\mathrm{NS}}(\theta) = \boldsymbol{\Xi}(\theta)\boldsymbol{\Phi}(\theta)$ and $\boldsymbol{J}\boldsymbol{a}_{\mathrm{NS}}^*(\theta) = \boldsymbol{\Xi}(\theta)\boldsymbol{\Lambda}(\theta)$, where

$$\boldsymbol{\Xi}(\theta) = \begin{bmatrix} \mathrm{e}^{(\mathrm{j}2\pi f\frac{d}{c}M\cos\theta)} & \cdots & 0 & \cdots & 0 \\ \vdots & \ddots & \vdots & \cdots & \vdots \\ 0 & \cdots & \mathrm{e}^{(\mathrm{j}2\pi f\frac{d}{c}m\cos\theta)} & \cdots & 0 \\ \vdots & \cdots & \vdots & \ddots & \vdots \\ 0 & \cdots & 0 & 0 & 1 \\ \vdots & \cdots & \vdots & \iddots & \vdots \\ 0 & \cdots & \mathrm{e}^{(-\mathrm{j}2\pi f\frac{d}{c}m\cos\theta)} & \cdots & 0 \\ \vdots & \iddots & \vdots & \cdots & \vdots \\ \mathrm{e}^{(-\mathrm{j}2\pi f\frac{d}{c}M\cos\theta)} & \cdots & 0 & \cdots & 0 \end{bmatrix}. \tag{43}$$

$$\boldsymbol{\Phi}(\theta) = \left[\exp\left(-\mathrm{j}2\pi f\left(\frac{M^2d^2}{4l_{n_2}c}\cos(2\theta) - \frac{M^2d^2}{4l_{n_2}c}\right)\right), \ldots, \exp\left(-\mathrm{j}2\pi f\left(\frac{m^2d^2}{4l_{n_2}c}\cos(2\theta) - \frac{m^2d^2}{4l_{n_2}c}\right)\right), \ldots, 1\right]^{\mathrm{T}} \tag{44}$$

$$\boldsymbol{\Lambda}(\theta)=\left[\exp\left(-\mathrm{j}2\pi f\left(\frac{-M^2d^2}{4l_{n_2}c}\cos(2\theta)+\frac{M^2d^2}{4l_{n_2}c}\right)\right), \ldots, \exp\left(-\mathrm{j}2\pi f\left(\frac{-m^2d^2}{4l_{n_2}c}\cos(2\theta) + \frac{m^2d^2}{4l_{n_2}c}\right)\right), \ldots, 1\right]^{\mathrm{T}}. \tag{45}$$

Combing (40) and (42), we have

$$\boldsymbol{a}_{\mathrm{NS}}^{\mathrm{H}}(\theta)\tilde{\boldsymbol{U}}\tilde{\boldsymbol{U}}^{\mathrm{H}}\boldsymbol{a}_{\mathrm{NS}}(\theta) = \boldsymbol{\Phi}^{\mathrm{H}}(\theta)\boldsymbol{\Xi}^{\mathrm{H}}(\theta)\tilde{\boldsymbol{U}}\tilde{\boldsymbol{U}}^{\mathrm{H}}\boldsymbol{\Xi}(\theta)\boldsymbol{\Phi}(\theta) = 0. \tag{46}$$

$$[\boldsymbol{J}\boldsymbol{a}_{\mathrm{NS}}^*(\theta)]^{\mathrm{H}}\tilde{\boldsymbol{U}}\tilde{\boldsymbol{U}}^{\mathrm{H}}[\boldsymbol{J}\boldsymbol{a}_{\mathrm{NS}}^*(\theta)] = \boldsymbol{\Lambda}^{\mathrm{H}}(\theta)\boldsymbol{\Xi}^{\mathrm{H}}(\theta)\tilde{\boldsymbol{U}}\tilde{\boldsymbol{U}}^{\mathrm{H}}\boldsymbol{\Xi}(\theta)\boldsymbol{\Lambda}(\theta) = 0. \tag{47}$$

Similarly, $\boldsymbol{\Phi}(\theta) \neq \mathbf{0}$ and $\boldsymbol{\Lambda}(\theta) \neq \mathbf{0}$, (46) and (47) hold only if $\boldsymbol{\Xi}^{\mathrm{H}}(\theta)\tilde{\boldsymbol{U}}\tilde{\boldsymbol{U}}^{\mathrm{H}}\boldsymbol{\Xi}(\theta)$ is singular, then we can obtain estimation of NS $\hat{\theta}_{N_1+1}, \ldots, \hat{\theta}_N$ by searching N_2 peaks of the equation below

$$P_{MU-N} = \frac{1}{|\boldsymbol{\Xi}^{\mathrm{H}}(\theta)\tilde{\boldsymbol{U}}\tilde{\boldsymbol{U}}^{\mathrm{H}}\boldsymbol{\Xi}(\theta)|}. \tag{48}$$

Besides, we know from Fig. 1, after acquiring DOA of NS, if there is no multi-path propagation, reflection or diffraction, the distance of $s_{n_2}(t)$ to the origin will also be estimated from $\boldsymbol{\Phi}(\theta)$ or $\boldsymbol{\Lambda}(\theta)$ according to (46) or (47). That means the locations of the signals can be determined. The method we propose is based on the calibration for the array, and it is suitable for mixed FS and NS, so it can be abbreviated as CFN method.

4. Computational complexity

Here, an eigenstructure method for estimating DOA and sensor gain-phase errors (AGP) [17], passive localization of mixed near-field and far-field sources using the two-stage MUSIC algorithm (PLT) [24], efficient application of the MUSIC algorithm under the coexistence of far-field and near-field sources (EAM) [26] and CFN are used for the comparison. Assume that the DOA of signals satisfy $0 < \eta_1 < \theta < \eta_2 < \pi$, searching step sizes of DOA and the distance are respectively Δ_θ and Δ_l. For convenience, we just compare the main steps, PLT and EAM both adapt to mixed FS and NS with ideal array, where PLT needs constructing one $(2M+1) \times (2M+1)$ and one $(4M+1) \times (4M+1)$ dimensional statistical matrices, eigen-decomposition, solving spatial spectrum, so the complexity of PLT is approximately $O\left(9(2M+1)^2Z+9(4M+1)^2Z+\frac{4}{3}(2M+1)^3+\frac{4}{3}(4M+1)^3+\frac{(\eta_2-\eta_1)(2M+1)^2}{\Delta_\theta}\right)$; EAM needs to form one $(2M+1)\times(2M+1)$ and one $(M+2)\times(M+2)$ dimensional statistical matrices, eigen-decomposition, solving spatial spectrum for DOA and the distance of NS, so it requires nearly $O\left((2M+1)^2Z + (M+2)^2M + \frac{4}{3}(2M+1)^3 + \frac{4}{3}(M+2)^3 + \frac{(\eta_2-\eta_1)(2M+1)^2}{\Delta_\theta} + \frac{(\eta_2-\eta_1)(M+2)^2}{\Delta_\theta} + N_2\frac{(2M+1)^2}{\Delta_l}\right)$; AGP adapts to FS and gain-phase calibration, it needs constructing statistical matrix, eigen-decomposition and solving spatial spectrum, so its complexity is almost $O\left((2M+1)^2Z + \frac{4}{3}(2M+1)^3 + \frac{(2M+1)^2}{\Delta_\theta}(\eta_2-\eta_1)^2 + \frac{(2M+1)^2}{\Delta_\theta}(\eta_2-\eta_1)\beta\right)$, where β indicates the iteration times; CFN involves computing $(2M+1) \times (2M+1)$ dimensional statistical matrices, eigen-decomposition and solving two one-dimensional spatial spectrums for FS and NS, so the complexity is about $O\bigg((2M+1)^2Z + \frac{8}{3}(2M+1)^3 +$

$$\left.\frac{2(\eta_2-\eta_1)(2M+1)^2}{\Delta_\theta}\right).$$

5. Simulations

In this section, some simulations are provided to prove these methods, consider some narrowband signals with the same power arriving at a uniform linear array composed of nine omnidirectional sensors, the fifth sensor is deemed to be the reference and origin, the structure is illustrated as Fig. 1. Three FS and three NS impinge on the array from $(73°, 79°, 85°)$ and $(40°, 55°, 65°)$ simultaneously, distances between the three NS and origin are respectively 10 m, 14 m and 18 m, their coordinates are defined as (x_{n_2}, y_{n_2}) $(n_2 = 1, 2, 3)$. The frequency of the signals is 0.1 GHz, and interspace between the sensors $d = \lambda/2$ =1.5 m. Here the gain and phase errors are generated by

$$\rho_m = 1 + \upsilon_\rho \xi_m, \varphi_m = \upsilon_\phi \zeta_m \tag{49}$$

where ξ_m and ζ_m are independent and identically distributed random variables in the uniform distribution over $[-0.5, 0.5]$, υ_ρ and υ_ϕ are the standard deviations of ρ_m and ϕ_m respectively, in simulation 5.1 – 5.5, define $\upsilon_\rho = 1$, $\upsilon_\phi = 64°$. We repeat 400 Monte-Carlo trials and their average is deemed to be the result. AGP, PLT, EAM and CFN are employed for the estimation, where AGP and CFN adapt to DOA estimation in the presence of gain-phase errors; PLT, EAM and CFN are suitable for mixed FS and NS. $\Delta_\theta = 0.2°$, $\Delta_l = 0.01$ m, iteration times of AGP $\beta = 500$.

5.1 DOA Estimation

Estimation error of FS is defined as $\sum\limits_{n_1=1}^{N_1} |\theta_{n_1} - \hat{\theta}_{n_1}|$, that of NS is defined as $\sum\limits_{n_2=1}^{N_2} |\theta_{n_2} - \hat{\theta}_{n_2}|$, Fig. 2 is the FS estimation errors versus signal-to-noise ratio (SNR) when number of snapshots is 70, Fig. 3 presents that versus number of snapshots when SNR is 8 dB.

We can see from Fig. 2 and Fig. 3, estimation accuracy of FS is improving with the increase of SNR or the number of snapshots, and all these methods are converged ultimately. As EAM and PLT are not suitable for the array calibration, there are still some errors even if SNR is high or the number of snapshots is large enough; AGP needs to cope with the gain-phase errors before estimating FS, this treatment also produces some uncertainties which will influence the final result; CFN avoids the process of calibration before calculating FS, so it manifests better than AGP and the other two methods.

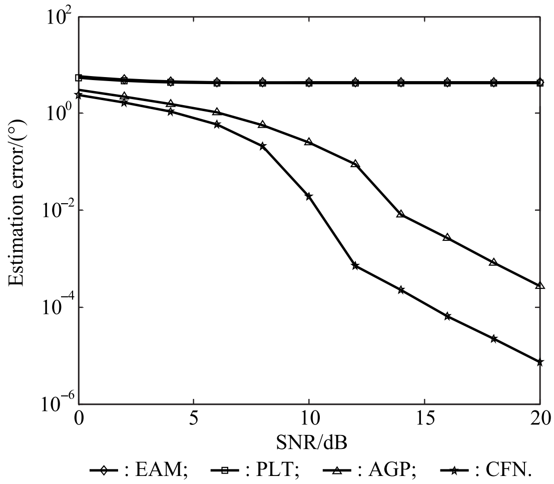

Fig. 2 DOA estimation errors of FS versus SNR

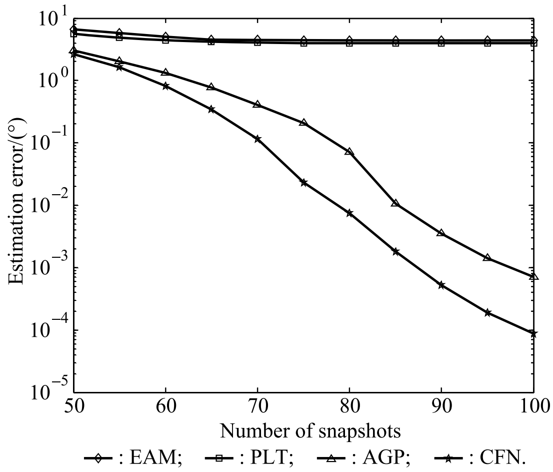

Fig. 3 DOA estimation errors of FS versus number of snapshots

Fig. 4 is the NS estimation errors versus SNR when the number of snapshots is 70, Fig. 5 demonstrates that versus number of snapshots when SNR is 8 dB.

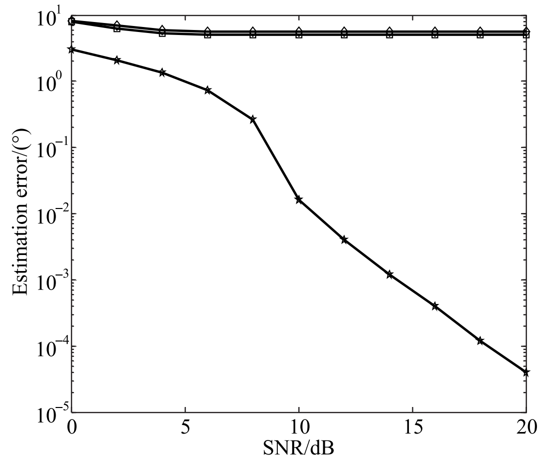

Fig. 4 DOA estimation errors of NS versus SNR

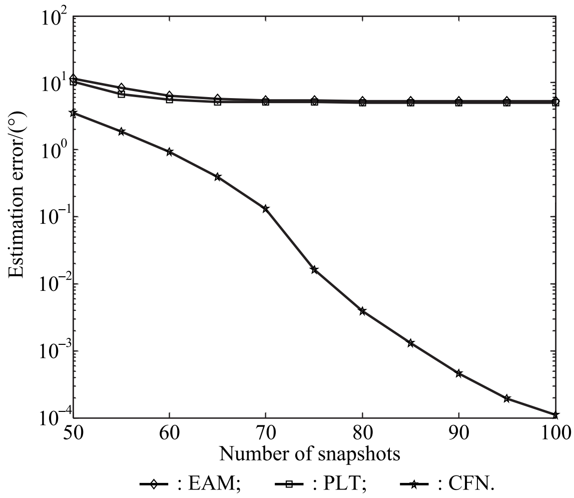

Fig. 5 DOA estimation errors of NS versus number of snapshots

From Fig. 4 and Fig. 5 we know that CFN is still effective to NS in the presence of gain-phase errors, while EAM and PLT have failed owing to the array errors.

5.2 Estimation for gain-phase errors

SNR is 6 dB, the number of snapshots is 30, other conditions are the same with 5.1, Fig. 6 and Fig. 7 respectively show the gain and phase error estimations of each sensor with AGP and CFN.

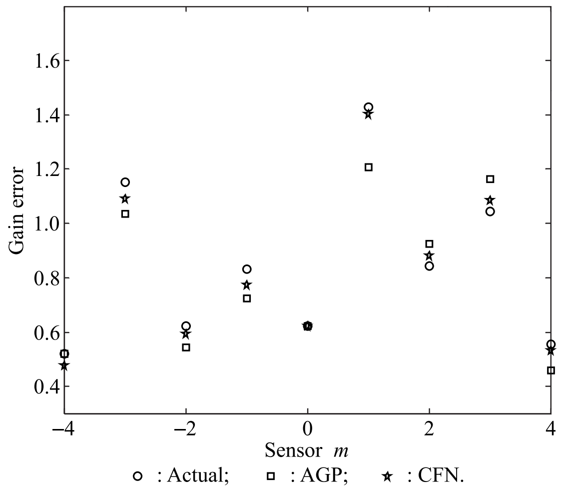

Fig. 6 Gain error estimation

We can see from Fig. 6 and Fig. 7, both AGP and CFN can estimate the gain and phase error of the array. The former method needs to calculate the noise variance before the gain error is determined. Moreover, AGP requires the condition that at least two signals are spatially far from each other when we compute their DOA which is needed in the course of solving the phase error [17]. Thus comparing with AGP, CFN is closer to the actual error in the case of low SNR, or signals are not far enough apart.

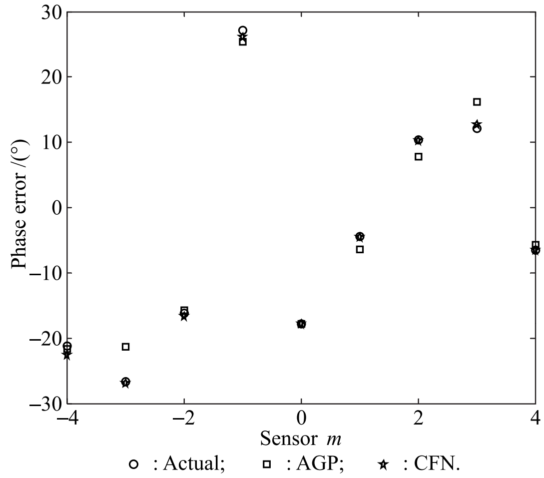

Fig. 7 Phase error estimation

5.3 Resolution capability for FS

Consider two FS arriving at the array from $(\vartheta_1, \vartheta_2)$ with the same power, here

$$P_{\mathrm{MUSIC}}\left(\frac{\vartheta_1+\vartheta_2}{2}\right) < \frac{P_{\mathrm{MUSIC}}(\vartheta_1)+P_{\mathrm{MUSIC}}(\vartheta_2)}{2}. \tag{50}$$

The two signals can be resolved, else they cannot [35], (49) represents there is hollowness between two spectrum peaks, and (21) is used as $P_{\mathrm{MUSIC}}(\,)$ for the CFN method.

In this simulation, consider two FS arriving at the array, their DOA are taken 90° as the symmetrical point, other conditions are the same with 5.2, the DOA interval is defined as $\Delta = |\vartheta_1 - \vartheta_2|$, 200 Monte-Carlo trials are repeated for each interval and we present the simulation result for resolution probability of success of two methods versus different DOA intervals, it is shown in Fig. 8.

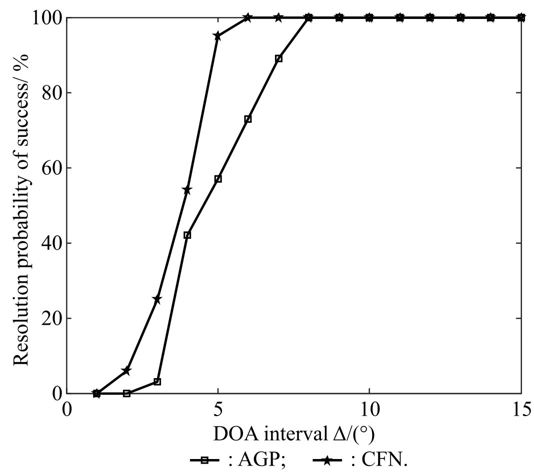

Fig. 8 Resolution capability versus different DOA intervals

From Fig. 8 it can be seen the resolution capability of CFN performs better than that of AGP when the two signals are close to each other, and the latter can not resolve them absolutely right until DOA interval is $8°$, after that there are no differences between the two methods.

5.4 Location for NS

Location error is defined as

$$\sum_{n_2=1}^{N_2} \sqrt{(x_{n_2} - \hat{x}_{n_2})^2 + (y_{n_2} - \hat{y}_{n_2})^2}$$

where (x_{n_2}, y_{n_2}) is the actual coordinate of $s_{n_2}(t)$, $(\hat{x}_{n_2}, \hat{y}_{n_2})$ is its corresponding estimation, SNR is 0 dB, the number of snapshots is 70, other conditions are the same with 5.1. Fig. 9 shows the estimated locations of the three NS. Fig. 10 presents the location errors versus SNR when the number of snapshots is 70.

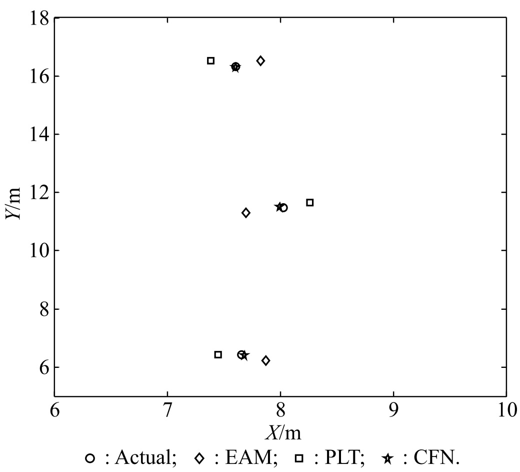

Fig. 9 Location estimation

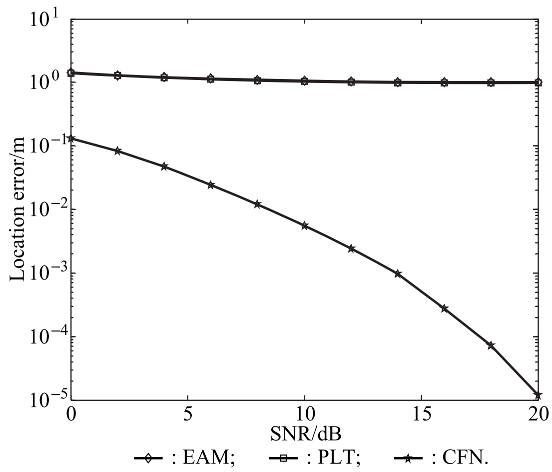

Fig. 10 Location errors versus SNR

It can be seen from Fig. 9, CFN can locate the signals relatively exactly, but EAM and PLT have failed because of the gain-phase errors. And we know from Fig. 10 that location estimations of the three methods are improving with the increase of SNR, in comparison, CFN can compute the location of NS more accurately. However, due to the array error, the other two methods still fail even if SNR is high enough.

5.5 Estimation for mixed signals with different powers

In this section, more complex scenarios will be considered, suppose that an FS and an NS with small DOA intervals arrive at the array simultaneously, we discuss the resolution of these methods. If DOA of the two mixed signals are respectively ϑ_F and ϑ_N, estimations of them are $\hat{\vartheta}_F$ and $\hat{\vartheta}_N$, if $|\vartheta_k - \hat{\vartheta}_k| < \dfrac{|\vartheta_F - \vartheta_N|}{2}$ $(k = F, N)$, we believe the two mixed signals can be resolved. In this simulation, $\vartheta_F = 93°$, $\vartheta_N = 87°$, SNR of FS is 0 dB, other conditions are the same with 5.4. Fig. 11 shows the resolution probability of success versus SNR of NS.

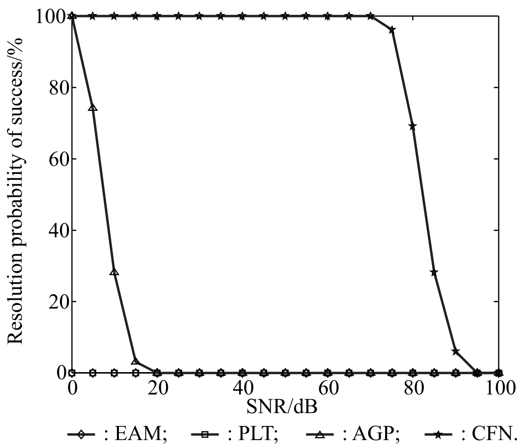

Fig. 11 Probability of success of mixed signals versus SNR disparity

It can be seen from Fig. 11, EAM and PLT cannot resolve the two signals from beginning to end because of the gain-phase errors. And when the power of NS is 70 dB higher than that of FS, CFN is still effective, when the SNR disparity is 95 dB, all these methods have failed completely. Therefore, even if the powers of the FS and NS with small DOA intervals are not the same, as long as they are not different from each other too much, the method we propose still applies here.

5.6 Estimation for NS versus gain-phase errors

It can be seen from the proposed method, FS estimation is independent of the gain-phase errors, so we only need to analyze the performance of NS versus gain-phase errors. In this simulation, SNR is 8 dB, the number of snapshots is 70, Fig. 12 shows the DOA estimation errors versus υ_ρ

when $\upsilon_\phi = 30°$. While Fig. 13 presents the DOA estimation errors versus υ_ϕ when $\upsilon_\rho = 0.2$.

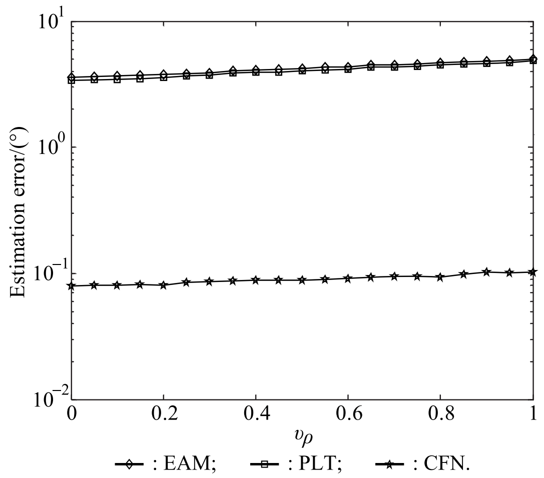

Fig. 12 DOA estimation error of NS versus gain error

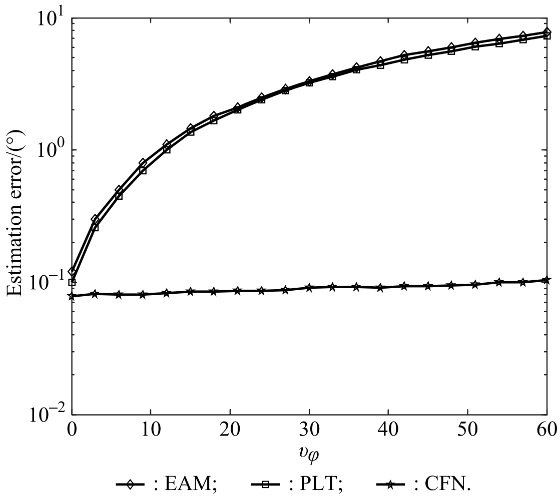

Fig. 13 DOA estimation error of NS versus phase error

It is noted that the performance of EAM and PLT degrades seriously as gain or phase error increases, and CFN is steady relatively, so the proposed method is applicable for gain-phase error array.

6. Conclusions

A novel approach of DOA estimation for mixed far-field and near-field signals based on gain-phase error array is proposed in the paper. It both adapts to mixed DOA estimation and location for near-field signals. Meanwhile, it changes two-dimensional spectrum searching into one-dimensional one by matrix transformation according to the special structure of the array, so as to improve the computational efficiency on the premise of ensuring a certain accuracy. However, it just applies to narrowband signals, we will be committed to studying the technique for wideband signals in future.

References

[1] X. H. Wang, J. F. Chen, J. Han. Optimization for the direction of arrival estimation based on single acoustic pressure gradient vector sensor. *International Journal of Naval Architecture and Ocean Engineering*, 2014, 6(1): 74 – 86.

[2] P. Palanisamy, N. Kalyanasundaram, P. M. Swetha. Two-dimensional DOA estimation of coherent signals using acoustic vector sensor array. *Signal Processing*, 2012, 92(1): 19 – 28.

[3] J. Y. Lee, R. E. Hudson, K. Yao. Acoustic DOA estimation: an approximate maximum likelihood approach. *IEEE Systems Journal*, 2014, 8(1): 131 – 141.

[4] D. M. P. Calderon, J. A. A. Jr. Shooter localization based on DOA estimation of gunshot signals and digital map information. *IEEE Latin America Transactions*, 2015, 13(2): 441 – 447.

[5] X. X. Cui, K. G. Yu, S. S. Lu. Direction finding for transient acoustic source based on biased TDOA measurement. *IEEE Trans. on Instrumentation and Measurement*, 2016, 65(11): 2442 – 2453.

[6] P. Tichavsky, K. T. Wong, M. D. Zoltowski. Near-field/far-field azimuth and elevation angle estimation using a single vector hydrophone. *IEEE Trans. on Signal Processing*, 2001, 49(11): 2498 – 2510.

[7] L. Sanchez, L. Munoz, J. A. Galache. Smart santander: IoT experimentation over a smart city testbed. *Computer Networks*, 2014, 61(14): 217 – 238.

[8] C. N. Verdouw, A. J. M. Beulens, J. G. A. J. Vandervorst. Virtualisation of floricultural supply chains: a review from an Internet of things perspective. *Computers and Electronics in Agriculture*, 2013, 99: 160 – 175.

[9] Y. Mohamedatni, B. Fergani, B. Laheurte. DOA estimation techniques applied to RFID tags using receiving uniform linear array. *Proc. of the IEEE International Symposium on Antenna and Propagation and USNC/URSI National Radio Science Meeting*, 2015: 1760 – 1761.

[10] G. Han, L. Wan, L. Shu. Two novel DOA estimation approaches for real-time assistant calibration systems in future vehicle industrial. *IEEE System Journal*, 2017, PP(99): 1 – 12.

[11] J. Li, Y. J. Zhao, D. H. Li. Accurate single-observer passive coherent location estimation based on TDOA and DOA. *Chinese Journal of Aeronautics*, 2014, 27(4): 913 – 923.

[12] G. Fabrizio, A. Heitmann. A multipath-driven approach to HF geolocation. *Signal Process*ing, 2013, 93(12): 3487 – 3503.

[13] J. Yang, W. J. Chen, L. Li. Long baseline direction finding and localization algorithms for noise radiation source. *Proc. of the 12th International Conference on Signal Processing*, 2014: 52 – 57.

[14] P. H. Leong, T. D. Abhayapala, T. A. Lamahewa. Multiple target localization using wideband echo chirp signals. *IEEE Trans. on Signal Processing*, 2013, 61(16): 4077 – 4089.

[15] G. Byun, H. Choo, H. Ling. Optimum placement of DF antenna elements for accurate DOA estimation in a harsh platform environment. *IEEE Trans. on Antennas and Propagation*, 2013, 61(9): 4783 – 4791.

[16] M. Biguesh. Bearing estimation using time delays: optimum sensor arrangement and an efficient estimator. *IEEE Sensors Journal*, 2016, 16(18): 6961 – 6965.

[17] A. F. Liu, G. S. Liao, C. Zeng. An eigenstructure method for estimating DOA and sensor gain-phase errors. *IEEE Trans. on Signal Processing*, 2011, 59(12): 5944 – 5956.

[18] H. W. Chen. Robustness analysis of nearfield subband beamformers in the presence of microphone gain and phase errors. *Digital Signal Processing*, 2013, 23(5): 1712 – 1719.

[19] A. Nikoofard, S. Kananian, F. A. Ali. A fully analog calibration technique for phase and gain mismatches in image-reject receivers. *International Journal of Electronics and Communications*, 2015, 69(5): 823 – 835.

[20] Z. Dai, W. M. Su, H. Gu. Sensor gain-phase errors estimation using disjoint sources in unknown directions. *IEEE Sensors Journal*, 2016, 16(10): 3724 – 3730.

[21] J. F. Li, X. F. Zhang, R. Z. Cao. Reduced-dimension MUSIC for angle and array gain-phase error estimation in bistatic MIMO radar. *IEEE Communications Letters*, 2013, 17(3): 443 – 446.

[22] J. F. Li, X. F. Zhang. A method for joint angle and array gain-phase error estimation in bistatic multiple-input multiple-output non-linear arrays. *IET Signal Processing*, 2014, 8(2): 131 – 137.

[23] J. Li, M. Jin, Y. Zheng. Transmit and receive array gain-phase error estimation in bistatic MIMO radar. *IEEE Antennas and Wireless Propagation Letters*, 2015, 14: 32 – 35.

[24] J. L. Liang, D. Liu. Passive localization of mixed near-field and far-field sources using two-stage MUSIC algorithm. *IEEE Trans. on Signal Processing*, 2010, 58(1): 108 – 120.

[25] B. Wang, J. J. Liu, X. Y. Sun. Mixed sources localization based on sparse signal reconstruction. *IEEE Signal Processing Letters*, 2012, 19(8): 487 – 490.

[26] J. He, M. N. S. Swamy, M. O. Ahmad. Efficient application of MUSIC algorithm under the coexistence of far-field and near-field sources. *IEEE Trans. on Signal Processing*, 2012, 60(4): 2066 – 2070.

[27] G. H. Liu, X. Y. Sun, Y. Y. Liu. Low-complexity estimation of signal parameters via rotational invariance techniques algorithm for mixed far-field and near-field cyclostationary sources localisation. *IET Signal Processing*, 2013, 7(5): 382 – 388.

[28] P. H. Leong, T. D. Abhayapala, T. A. Lamahewa. Multiple 3D far-field /near-field moving target localization using wideband echo chirp signals. *IEEE Trans. on Signal Processing*, 2014, 62(22): 6003 – 6015.

[29] L. Zhang, J. D. Mei, A. Zielinski. Direction-of-arrival estimation for far-field acoustic signal in presence of near-field interferences. *Electronics Letters*, 2015, 51(1): 101 – 103.

[30] K. Wang, L. Wang, J. R. Shang. Mixed near-field and far-field source localization based on uniform linear array partition. *IEEE Sensors Journal*, 2016, 16(22): 8083 – 8090.

[31] O. Malyuskin, V. F. Fusco. Ultracompact retrodirective antenna arrays with superdirective radiation patterns. *IEEE Trans. on Antennas and Propagation*, 2016, 64(7): 2923 – 2935.

[32] P. E. B. Jourdain. The influence of Fourier's theory of the conduction of heat on the development of pure mathematics. *Scientia*, 1917, 11(2): 245 – 246.

[33] R. O. Schmidt. Multiple emitter location and signal parameter estimation. *IEEE Trans. on Antennas and Propagation*, 1986, 34(3): 276 – 280.

[34] S. Prasad, R. T. Williams, A. K. Mahalanabis. A transform-based covariance differencing approach for some classes of parameter estimation problems. *IEEE Trans. on Acoustics, Speech, and Signal Processing*, 1988, 36(5): 631 – 641.

[35] C. G. Zhou, F. Haber, D. L. Jaggard. A resolution measure for the MUSIC algorithm and its application to plane wave arrivals contaminated by coherent interference. *IEEE Trans. on Signal Processing*, 1991, 39(2): 454 – 463.

Biographies

Jiaqi Zhen was born in 1981. He received his Ph.D. degree in academic of communication engineering from Harbin Engineering University in 2011. He is currently an associate professor at the College of Electronic Engineering in Heilongjiang University, Heilongjiang, China. His current research interest is array signal processing.
E-mail: zhenjiaqi2011@163.com

Yong Liu was born in 1970. He received his bachelor's degree in College of Electronic Engineering, Heilongjiang University in 1993. He is currently an associate professor at the College of Electronic Engineering in Heilongjiang University, Heilongjiang, China. His current research interest is communication signal processing.
E-mail: 156083143@qq.com